Accident Analysis and Prevention 117 (2018) 346–356

Contents lists available at ScienceDirect

Accident Analysis and Prevention

journal homepage: www.elsevier.com/locate/aap

Key risk indicators for accident assessment conditioned on pre-crash vehicle trajectory

X. Shi[a,*], Y.D. Wong[a], M.Z.F. Li[b], C. Chai[c]

[a] School of Civil & Environmental Engineering, Nanyang Technological University, 639798, Singapore
[b] Nanyang Business School, Nanyang Technological University, 639798, Singapore
[c] College of Transportation Engineering, Tongji University, 201804, China

ARTICLE INFO

Keywords:
Key risk indicator
Risk exposure
Pre-accident risk
Vehicle risk

ABSTRACT

Accident events are generally unexpected and occur rarely. Pre-accident risk assessment by surrogate indicators is an effective way to identify risk levels and thus boost accident prediction. Herein, the concept of Key Risk Indicator (KRI) is proposed, which assesses risk exposures using hybrid indicators. Seven metrics are shortlisted as the basic indicators in KRI, with evaluation in terms of risk behaviour, risk avoidance, and risk margin. A typical real-world chain-collision accident and its antecedent (pre-crash) road traffic movements are retrieved from surveillance video footage, and a grid remapping method is proposed for data extraction and coordinates transformation. To investigate the feasibility of each indicator in risk assessment, a temporal-spatial case-control is designed. By comparison, Time Integrated Time-to-collision (TIT) performs better in identifying pre-accident risk conditions; while Crash Potential Index (CPI) is helpful in further picking out the severest ones (the near-accident). Based on TIT and CPI, the expressions of KRIs are developed, which enable us to evaluate risk severity with three levels, as well as the likelihood. KRI-based risk assessment also reveals predictive insights about a potential accident, including at-risk vehicles, locations and time. Furthermore, straightforward thresholds are defined flexibly in KRIs, since the impact of different threshold values is found not to be very critical. For better validation, another independent real-world accident sample is examined, and the two results are in close agreement. Hierarchical indicators such as KRIs offer new insights about pre-accident risk exposures, which is helpful for accident assessment and prediction.

1. Introduction

Traffic accidents cause great loss of lives and property damage. Reliable accident prediction and proactive prevention are undoubtedly of great benefit and necessity.

Numerous studies have been conducted on traffic accident assessment and prevention. Accident occurrence is a complex mechanism, with many contributing factors (Mannering et al., 2016). Unsafe traffic conditions and risky driving behaviours have been explored to characterise accidents, including human errors, traffic speed and occupancy, weather and visibility (e.g. Saifuzzaman and Zheng, 2014; Young, 2017). Statistical models and machine learning approaches are being widely applied to analyse the relationship between accidents and influencing factors, such as random forests (Abdel-Aty and Haleem, 2011), support vector machine (Dong et al., 2015), among others. These studies are helpful to describe general linkages between accident numbers and coexisting factors or concurrent scenarios. Nevertheless, even under equivalent situations, actual accident occurrence remains unreliable to be assessed or predicted if merely relying on these trends and factors. Due to uncertainty and randomness, effective accident assessment and prediction has been found to be extremely difficult.

Risk assessment is essential when making any accident prediction. Pre-accident risk exposure is more meaningful for accident prediction and prevention. Although the occurrence of an accident is generally unexpected, for certain types of accidents, there is an accident-forming process, especially for accidents associated with traffic conflicts. Traffic conflict represents a transitional state between safety and a potential accident. A conflict is an observed situation in which two or more road users approach each other in space and time to such an extent that there is a risk of collision if their movements remain unchanged (Amundsen and Hydén, 1977). Conflicts can improve the understanding of the accident mechanism and chain of events which may lead to a collision (Mahmud et al., 2017). Compared with actual accidents, incidences of traffic conflicts, with attendant collision risks of various degrees, are more frequent (Chin and Quek, 1997). Moreover, a strong relationship has been found between traffic conflicts and actual crashes in many

* Corresponding author.
E-mail addresses: XSHI004@e.ntu.edu.sg (X. Shi), CYDWONG@ntu.edu.sg (Y.D. Wong), ZFLI@ntu.edu.sg (M.Z.F. Li), chaichen@tongji.edu.cn (C. Chai).

https://doi.org/10.1016/j.aap.2018.05.007
Received 27 December 2017; Received in revised form 4 May 2018; Accepted 7 May 2018
Available online 14 May 2018
0001-4575/

studies (e.g. El-Basyouny and Sayed, 2013, Wu et al., 2014). Herein, the scope of risk assessment should therefore focus on pre-accident traffic conflicts, as an alternative to actual accident numbers.

Surrogate measures are widely utilised in traffic conflict techniques (TCT) for safety evaluation (e.g. Zheng et al., 2014). Mahmud et al. (2017) provides a comprehensive review on the developments and applications of 17 proximal surrogate indicators. The reliability and validity of surrogate indicators are well accepted for safety evaluation (Chai and Wong, 2015). In practice, FHWA developed a Surrogate Safety Assessment Model (SSAM) as a post processor to determine the number and severity of conflicts obtained from simulation packages (Sobhani et al., 2013). Many advanced driving assistance systems (ADAS) have used surrogate indicators as important warning criteria (Wang et al., 2013). Nevertheless, the effectiveness of surrogate indicators under real-world accidents has not been properly investigated. In particular, it remains unclear the extent to which the surrogate indicators are useful for pre-accident risk assessment. Besides, indicators are often designed under simplified assumptions, such as unchanged trajectory, constant speed and predefined deceleration rate. To represent complex accident mechanism, combined use of various indicators has been suggested (e.g. Laureshyn et al., 2010). However, no consensus has been reached yet on which indicators should be selected and how to combine them.

High-quality data is necessary for risk measurement. Existing studies widely use accident data from police recording and self-reports, controlled experiments and simulation, loop detectors, etc. From such sources, it is extremely difficult to obtain pre-accident data of high-quality (e.g. accurate, 1-s resolution or less, vehicle level) (Imprialou and Quddus, 2017). Besides, real-world accidents are generally unexpected and occur rarely, and purposive tracking is very costly (Hakkert and Gitelman, 2014). Note that it is near impossible to pinpoint the precise time and location of an accident before-hand. Herein, a practical way to obtain pre-accident information is by retrieving the video footage that contains an accident event. Such video footage can be gathered by a surveillance camera system that continuously records traffic movements for the entire road network.

However, data extraction from video recording is also challenging. Existing methods in computer vision are useful for vehicle detection and tracking (e.g. vehicle/non-vehicle classification, vehicle counting) (e.g. Sivaraman and Trivedi, 2013), but they are problematic for accurate data extraction and measurement (e.g. vehicle trajectory, gap, speed). Additionally, there are many constraints in camera-based data acquisition, such as lens distortion from camera angles, object overlapping in dense conditions. The solution for exact measurement is lacking. Chai and Wong (2013) developed and applied a technique of measuring a vehicle trajectory by a projective transformation of video frames at first, and then indicating vehicle positions by means of computer-aided annotation; this hybrid approach is flexible and easy to use, albeit involving certain tedium.

Being different from previous studies in the literature, this paper focuses on developing hybrid indicators, namely the key risk indicators (KRIs), to hierarchically assess pre-accident risk exposures. Section 2 develops the concept of KRI, and elaborates the selection of basic indicators. Section 3 describes the data extraction of pre-accident vehicle trajectory, and proposes a grid remapping method for coordinates transformation. Section 4 constructs the KRIs based on the findings from a spatial-temporal case-control and conducts the validation by another accident event. The final two sections cover the discussion and conclusion.

2. Concept of key risk indicator

2.1. Introduction of KRI

The concept of KRI has important applications in several areas, such as operational risk management (Scandizzo, 2005) and enterprise risk management (ERM) (Hwang et al., 2010) and financing, among others.

As applied to road safety, KRIs are metrics capable of revealing risk exposures in traffic flow, and providing predictive signals of a potential accident. KRIs enable us to identify risks that may lead to an accident, and grasp insights of an impending accident (such as at-risk vehicles, potential locations and time), thus the prevention strategy can be applied in a targeted and pre-emptive way. Hence, for accident assessment and prediction purposes, it is crucial that KRIs are designed effectively and reliably.

KRIs are developed based on a set of basic indicators that are effective and reliable in measuring risks. The design of KRIs starts with first shortlisting a set of existing metrics and then identifying the most critical ones that can serve as the basic indicators. The guiding principles for selecting metrics are outlined, such as meaningfulness, measurability, predictability (e.g. leading indicators), etc. Shortlisted metrics should offer useful insights about accident risks and be easy and clear to interpret. Complex metrics would make it difficult to track and manage. In addition, leading indicators should be included to offer predictive signals of a potential accident.

2.2. Risk behaviour indicators

Driving behaviour plays a major role in accident risk. High-risk driving behaviours may result in high likelihood of an accident, such as excessive speeding, driving too close to the preceding vehicle, etc. As a result, temporal and spatial proximity can be used to evaluate such risk behaviours. In addition, indicators based on temporal proximity are relatively popular and objective, because they integrate both the spatial proximity and speed difference (Zheng et al., 2014). Among time-based indicators, Time to Collision (TTC) is well-recognised and widely-used in practice, for theoretical and reliability reasons (Mahmud et al., 2017). Based on TTC, Time Exposed TTC (TET) and Time Integrated TTC (TIT) were further proposed (Minderhoud and Bovy, 2001), to measure risk duration and risk integration, respectively. The three time-based indicators are shortlisted.

(1) The basic TTC is defined by the time to a potential collision between two vehicles (van der Horst, 1990), as follows:

$$TTC_i(t) = \begin{cases} \frac{X_{i-1}(t) - X_i(t) - L_{i-1}}{V_i(t) - V_{i-1}(t)} & V_i(t) > V_{i-1}(t) \\ \infty & V_i(t) \le V_{i-1}(t) \end{cases}$$

where $x_i(t)$ and $v_i(t)$ are the position and velocity of targeted (following) vehicle (i) at timestamp t, and L_{i-1} is the length of preceding (leading) vehicle ($i-1$).

Generally, risk behaviours are flagged for any vehicle pair with a TTC value less than a given threshold. However, risk severity associated with TTC is not obvious. TTC notion is illustrated with vehicle trajectories in Fig. 1(a).

(2) TET expresses the total time of a vehicle exposed in risk situations, as follows:

$$TET_i = \sum_{t=0}^{N} \delta_i(t) \cdot \tau_{sc}$$

$$\delta_i(t) = \begin{cases} 1 & \forall \ 0 \le TTC_i(t) \le TTC^* \\ 0 & otherwise \end{cases}$$

where, for a period $T = N \bullet \tau_{sc}$, there are N small time intervals, each interval is τ_{sc} (e.g. 0.1 s). $\delta_i(t)$ is a switching variable between 1 and 0, and value 1 indicates a signal of risk condition, when the TTC value is below threshold TTC*.

(3) TIT takes into account the accumulated impact of risk behaviour, using integration of TTC profile below specified threshold, as follows:

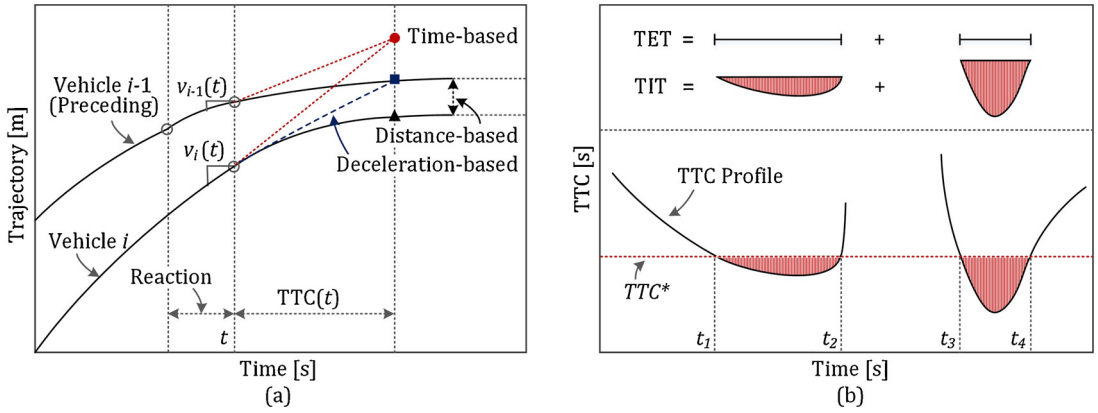

Fig. 1. Graphical representation of the indicators.

$$TIT_i = \sum_{t=0}^{N} [TTC^* - TTC_i(t)] \cdot \tau_{sc}$$
$$\forall\ 0 \le TTC_i(t) \le TTC^*$$

TIT suggests a risk accumulation in both risk severity and exposure duration. The graphical representation of TET and TIT is shown in Fig. 1(b) (adapted from Minderhoud and Bovy, 2001).

2.3. Risk avoidance indicators

The likelihood of an accident also depends on risk avoidance. A hazard condition that is hard to eliminate also indicates a high level of risk severity. The distinction between a crash and a near-miss depends on the evasive manoeuvres, such as timely reaction and required braking. A vehicle collision could be avoided if the following vehicle timely decelerated to stop or matched the speed of leading vehicle. Herein, two deceleration-based indicators are introduced to evaluate kinematic characteristics involving risk avoidance. Deceleration rate to avoid crash (DRAC) is recognised as a safety performance indicator, as it explicitly considers the role of differential speeds and decelerations in risk avoidance (Archer, 2005). Based on DRAC, an improved indicator was proposed, namely crash potential index (CPI), which considers many major factors in risk avoidance, including available braking capacity and time exposed to risk (Cunto and Saccomanno, 2008).

(1) DRAC evaluates the braking requirement during a vehicle conflict, which is represented by the minimum deceleration rate required to avoid the collision, as follows:

$$DRAC_i(t) = \begin{cases} \frac{[v_i(t) - v_{i-1}(t)]^2}{x_{i-1}(t) - x_i(t) - L_{i-1}} & v_i(t) > v_{i-1}(t) \\ 0 & v_i(t) \le v_{i-1}(t) \end{cases}$$

(2) CPI measures the probability that a vehicle's DRAC exceeds its maximum available deceleration rate (MADR) or braking capacity during a given period, as follows:

$$CPI_i = \frac{\sum_{t=0}^{N} p(DRAC_i(t) > MADR^{(\alpha_1, \alpha_2, \ldots, \alpha_n)}) \cdot \tau_{sc}}{T}$$

MADR is specific for a given set of traffic and environmental attributes ($\alpha_1, \alpha_2, \cdots, \alpha_n$), and depends on factors such as pavement conditions (e.g. dry, wet, snow), vehicle weight (e.g. car, truck) and braking system (Cunto and Saccomanno, 2008).

2.4. Risk margin indicators

Some accidents are triggered under exceptional circumstances, such as an abrupt hazard in front, driver cognitive failures and driving errors (Chai et al., 2017). For spatial proximity in emergency risks, the time-based indicators are not sensitive, and maximum braking capacity is generally applied. Accident risk is high if the available space is smaller than the space needed for an evasive reaction. Herein, distance-based indicators are suitable to measure the accident risks associated with emergencies by spatial characteristics. Proportion of stopping sight distance (PSD) measures the risk margin to the potential point of accident. Similarly, potential index for collision with urgent deceleration (PICUD) evaluates the risk margin under emergency braking. Besides, PICUD is helpful to evaluate two vehicles with similar speeds and the effect of gap keeping.

(1) PSD is the ratio of remaining distance (RD) to the potential point of accident and acceptable minimum stopping distance (MSD) (Allen et al., 1978), as follows:

$$PSD = {RD}/{MSD}\ ,\quad MSD = {v_i(t)^2}/{2d}$$

where d is acceptable maximum deceleration rate.

(2) PICUD is defined as the distance between two consecutive vehicles when they completely stop under emergency braking (Uno et al., 2003), as follows:

$$PICUD = \frac{v_{i-1}(t)^2 - v_i(t)^2}{2\alpha} + s_0 - v_i(t) \cdot \Delta t$$

where α is deceleration rate, s_0 is the initial distance, Δt is driver's reaction time.

These seven basic indicators are as shortlisted above. More information about them is described in Appendix A. The suitability and effectiveness of each indicator will be assessed based on real-world accident data, and findings shall serve as proof-of-concept in applying KRIs for accident assessment and prediction.

3. Pre-accident data acquisition

3.1. Accident data retrieval

To evaluate the indicator performance in pre-accident risk assessment, a typical real-world traffic accident involving multiple-vehicle collision is selected for data extraction. The particular accident occurred on the fastest lane (right-most) of a straight, level segment of an expressway carriageway during morning peak hours. The accident was captured by the expressway surveillance system of Land Transport Authority (LTA) Singapore. The surveillance camera is on fixed settings. Video footage of the main accident process and 1-min antecedent (pre-crash) road traffic movements is used. Images are extracted from the

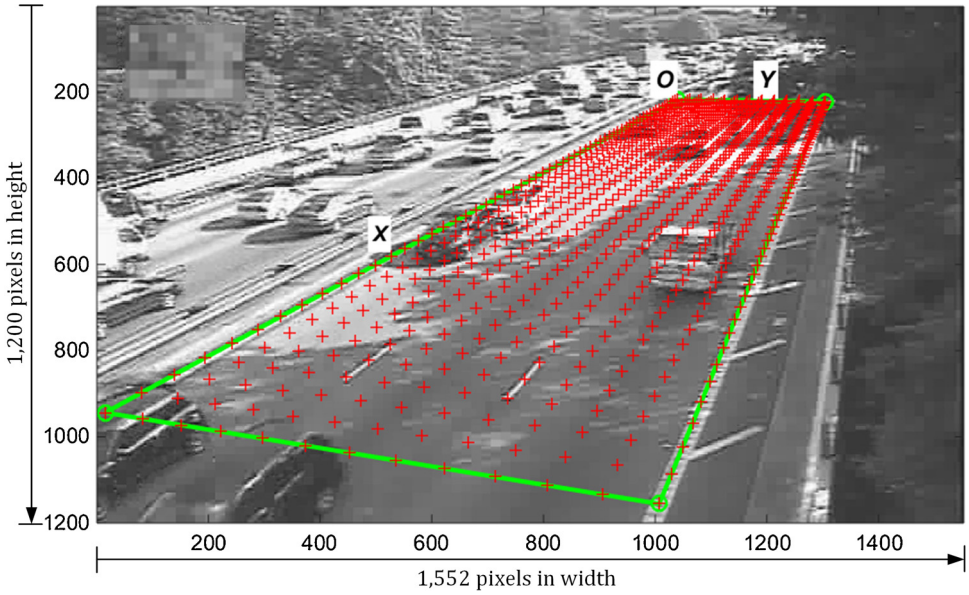

Fig. 2. Surveillance camera coverage and grid remapping area.

video footage at a sampling rate of one frame per 0.5 s. Each image has a resolution of 1552 pixels in width and 1200 pixels in height, as shown in Fig. 2.

3.2. Image-based data extraction

The extraction of vehicle trajectory data from video images is conducted by computer-aided vehicle detection. This method relies on manually detecting the vehicle's trajectory point and automatically recording the pixel coordinates of the detected point. The pixel coordinates (x_i^p, y_i^p) locate a pixel in an image array, where x_i^p is the column index value and is the row index value. The pixel indices are ordered from top to bottom and left to right, as illustrated by Fig. 2. The centre of the vehicle's front number plate is used as the detected point. Vehicle length is measured by the distance between headlight and corresponding rear-light. The vehicle detection and trajectory labelling by pixel coordinates are illustrated in Fig. 3(a).

3.3. Coordinates transformation

The extracted data is described by pixel coordinates in the image space, which needs to be transformed into coordinates described by real-world units (e.g. metres). Moreover, due to camera view, there is obvious lens distortion and irregular scaling. To accurately measure trajectory in real-world units, a grid remapping method is developed with three steps, namely grid mesh establishment, vehicle remapping and in-cell measurement.

(1) Grid mesh establishment based on camera calibration

The grid mesh is established by dividing the road segment on the image into many counting cells. Every cell is of equal size in real-world units, which represents an equal-sized planar area on the actual road. The grid mesh with equal-sized cells is generated by implementing the camera calibration algorithm proposed by Zhang (2000, 2004), which is widely applied and flexible to use.

Firstly, a remapping area is identified from real-world road segment. The remapping area is on regular and conformal setting, as illustrated in Fig. 3(b). Such setting is helpful to restore the parallel geometric relationship and consequently reduces the impact of lens distortion. In this case, a rectangular remapping area is selected based on parallel road markings, as illustrated in Fig. 2.

Secondly, the vertices of the remapping area are marked on the image space. The four vertices are set up to determine the projection relationship between real-world and image space, as illustrated in Figs. 2 and 3(b).

Lastly, the grid mesh is generated based on the four vertices using Zhang's camera calibration algorithm. The grid mesh consists of equal-sized counting cells, as showed in Fig. 3(c). Every cell has a corresponding distortion as the object in image space does. The configuration of the grid mesh is related to the layout of observed road segment, as well as video camera position and angle of view.

(2) Vehicle remapping

This step is to estimate an approximate value of trajectory coordinates by mapping vehicles onto corresponding cells in grid mesh system. Each grid cell has a unique address $(x_i^c(t), y_i^c(t))$, which is measured by the counting indices from the base point. The base point is set as the top-left vertex of the grid mesh system, thus the x-axis is along the right-most edge of road section in the direction of vehicle travel, and the y-axis is along the baseline, as illustrated in Figs. 2 and 3(c). Hence, the cell address is a binary variable estimation of vehicle coordinates.

The vehicle remapping is a matching between the grid cell and the labelled vehicle, by judging whether the trajectory point P: $(x_i^p(t), y_i^p(t))$ is located within the cell C: (n, m) or not, as shown in following:

$$F_{inpolygon}((x_i^p(t), y_i^p(t))(n, m)) = \begin{cases} 1 & if\ pixel\ in\ cell \\ 0 & otherwise \end{cases}$$

$$\forall\ F_{inpolygon} = 1,\ (x_i^c(t), y_i^c(t)) = (n, m)$$

$$\Rightarrow (x_i^p(t), y_i^p(t)) \leftrightarrow (x_i^c(t), y_i^c(t))$$

The cell C: (n, m) is a quadrilateral region whose four vertices are specified by pixel coordinates (x_{n-1}^p, y_{m-1}^p), (x_{n-1}^p, y_m^p), (x_n^p, y_{m-1}^p), and (x_n^p, y_m^p), as illustrated in Fig. 3(d). If the trajectory point is inside or on the edge of the quadrilateral cell region, $F_{inpolygon} = 1$. The inpolygon function is based on the algorithm for point in polygon proposed by Hormann and Agathos (2001). Herein, an approximate value of vehicle

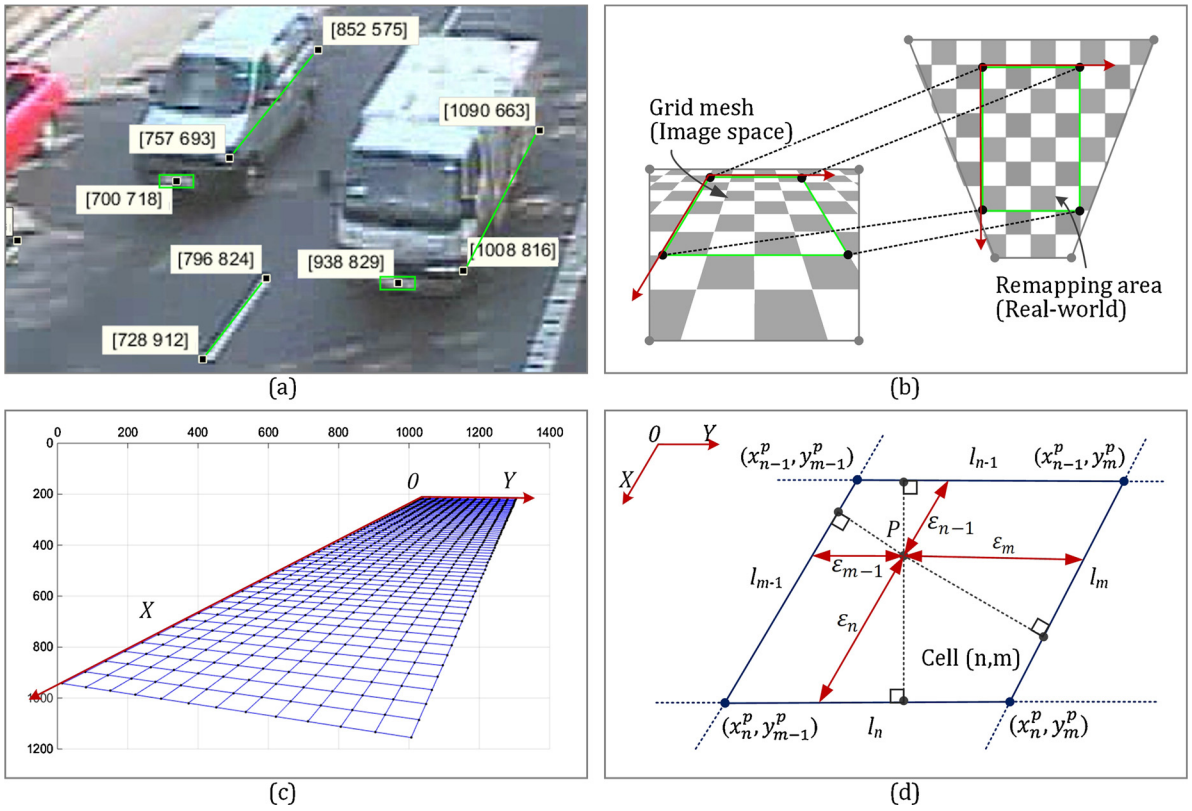

Fig. 3. Vehicle detection and trajectory measurement.

trajectory is described by the cell address $(x_i^c(t), y_i^c(t))$ under the grid mesh system.

(3) In-cell measurement

This step is to measure more accurate trajectory coordinates by calculating detailed in-cell position. The cell address and in-cell position further form into detailed grid coordinates. The calculation of trajectory coordinates is shown in following:

$$\underbrace{(x_i^g(t), y_i^g(t))}_{\text{Grid coordinates}} = \underbrace{(x_i^c(t), y_i^c(t))}_{\text{Cell address}} - \underbrace{(x_i^\varepsilon(t), y_i^\varepsilon(t))}_{\text{In-cell position}}$$

$$(x_i(t), y_i(t)) = (x_i^g(t)\cdot s_x, y_i^g(t)\cdot s_y)$$

$$(x_i^\varepsilon(t), y_i^\varepsilon(t)) = \left(\frac{\varepsilon_m}{\varepsilon_m + \varepsilon_{m-1}}, \frac{\varepsilon_n}{\varepsilon_n + \varepsilon_{n-1}}\right)$$

$$\frac{\varepsilon_m}{\varepsilon_m + \varepsilon_{m-1}} \cong \frac{D(P, l_m)}{D(P, l_m) + D(P, l_{m-1})}$$

where variables ε_m and ε_n are the in-cell proportions as illustrated in Fig. 3(d). Since each cell is approximately a parallelogram, the in-cell proportions can be measured based on the point-line distance $D(P, l)$. Note that the trajectory coordinates $(x_i(t), y_i(t))$ in real-world units are obtained based on grid coordinates and conversion coefficients, s_x and s_y.

The conversion of the cell size into real-world units is determined by the relationship between grid mesh structure and corresponding real-world coverage. In this case, a 60 × 12 grid mesh structure is used to cover the remapping area with 720 counting cells. The remapping area is about 60 m in length and with width of 3 lanes. Each lane in this road section is 3.7 m in width. Herein, the corresponding real-world size of the 60 × 12 grid mesh is 60 m by 11.1 m. Thus, the conversion coefficients are 1.0 m/cell in length (s_x) and 0.925 m/cell in width (s_y).

3.4. Calibration and verification

The proposed grid remapping method is feasible and practical to solve the problems of image-based data extraction and coordinates transformation. To ensure high-accuracy, the configuration of the rectangle remapping area should be convenient for real-world scale measurement, and with vertices to be clearly identified on image. Herein, an on-site survey of the remapping area would be helpful. To mitigate errors derived from lens distortion, a smaller cell size is recommended, for instance, no greater than 1.0 metre/cell. Besides, the vehicles in far view are blurred for observation, therefore, only data from the foreground 50 m road segment is used in subsequent analysis.

Verification is conducted by comparing the results with real-world targets. Targets with known size are used to check the accuracy, such as road surface markings and lines, known car length. In this case, the lane marking between lanes on expressway is used for checking. According to LTA standard on the details of road elements, the length of the dashed white lane marking is 2.0 m. For the lane marking in Fig. 3(a), pixel coordinates (728, 912) and (796, 824) are converted to be (57.06, 7.95) and (54.98, 8.07), respectively. Thus, the result is 2.08 m long, with an accuracy of 96%. To achieve a reliable measurement, an iterative process in terms of grid mesh estimation and remapping configuration is performed based on the discrepancies between the results and actual values, until the accuracy becomes acceptable. Compared with existing solutions, grid remapping method has a good performance in both accuracy and efficiency.

4. KRIs for a real accident assessment

4.1. Pre-accident reconstruction

The pre-accident scenario is reconstructed to investigate factors that

Table 1
Temporal-spatial case-control comparison.

Groups	Case [a]	Temporal Controls			Spatial Controls	
		[b]	[c]	[d]	[e]	[f]
Accident	Yes	No	No	No	No	No
Lane	Fast	Fast	Fast	Fast	Middle	Slow
Time segment (s)	33–42.5	23–32.5	13–22.5	3–12.5	33–42.5	33–42.5
Traffic flow information						
Vehicle count[a]	8	9	9	8	9	6
Mean speed (km/h)	49.2	51.9	51.7	37.0	68.7	54.1
S.D. of speed	9.0	10.2	12.3	4.6	14.5	7.5
Mean front gap (m)	14.5	16.0	14.8	12.3	15.7	20.4
S.D. of front gap	8.8	6.3	8.0	5.2	11.4	10.7
TTC						
No. of at-risk vehicles[b]	4	1	0	1	0	0
Exposure time (s)	4.0	0.5	0	0.5	0	0
Average TTC (s)	1.63	2.05	–	3.45	–	–
Min TTC (s)	0.50	2.05	6.60	3.45	4.19	5.79
TET						
TTC* = 1.5 s	1.5	0	0	0	0	0
TTC* = 2.0 s	3.0	0	0	0	0	0
TTC* = 2.5 s	3.5	0.5	0	0	0	0
TTC* = 3.0 s	3.5	0.5	0	0	0	0
TTC* = 3.5 s	4.0	0.5	0	0.5	0	0
TTC* = 4.0 s	4.0	0.5	0	0.5	0	0
TIT						
TTC* = 1.5 s	1.08	0	0	0	0	0
TTC* = 2.0 s	2.20	0	0	0	0	0
TTC* = 2.5 s	3.72	0.22	0	0	0	0
TTC* = 3.0 s	5.47	0.47	0	0	0	0
TTC* = 3.5 s	7.47	0.72	0	0.02	0	0
TTC* = 4.0 s	9.47	0.97	0	0.27	0	0
DRAC						
No. of at-risk vehicles	3	0	0	0	1	0
Exposure time (s)	1.5	0	0	0	0.5	0
Average DRAC (m/s^2)	6.24	–	–	–	3.83	–
Max DRAC (m/s^2)	7.51	–	–	–	3.83	–
CPI						
MADR1	0.06	0	0	0	0.02	0
MADR2	0.33	0	0	0	0	0
PSD						
No. of at-risk vehicles	6	4	2	1	1	1
Exposure time (s)	5.5	2.5	1.5	1.5	0.5	0.5
Average PSD	0.68	0.79	0.90	0.88	0.80	0.85
PICUD						
No. of at-risk vehicles	8	6	4	3	5	2
Exposure time (s)	7.5	4.0	4.0	3.0	3.5	2.5
Average PICUD (m)	−18.2	−14.4	−9.6	−4.4	−6.8	−4.5

[a] Number of vehicles contained within observation window of each group.
[b] Based on TTC threshold value of 4.0 herein, as a demonstration.
* Different TTC threshold values, for testing threshold sensitivity.

might cause/affect the accident. The four-vehicle head-to-rear collision occurred at the 43rd second on the fast lane. For the fast lane, there were 29 vehicles that passed through the 50-m road segment over 45 s (43-s pre-accident and 2-s post-accident), therein, five vehicles were highly relevant to the accident. Initially, several vehicles were moving fast with short front gaps, which reflected an unsafe condition existing in the dense traffic flow. At about the 39th second, a vehicle (Vehicle ID: 24) made an urgent deceleration, triggering a high-risk condition. The following vehicles (Vehicle IDs from 25 to 29) sequentially responded with deceleration, however, vehicle 27 failed in risk avoidance and hit the rear of vehicle 26, causing the accident. Furthermore, vehicles 28 and 29 also failed to stop before the accident point and were thus involved in this chain collision.

The pre-accident reconstruction reflects several major contributing factors to the accident, including unsafe driving behaviour (e.g. high speed with short gap in dense flow), high-risk conditions (e.g. urgent deceleration, abrupt collision in front), failure of collision avoidance (e.g. braking capacity, stop before the accident point), etc.

4.2. Temporal-spatial case-control

A temporal-spatial case-control study is designed to evaluate the indicators for pre-accident risk assessment. The case-control design contains one accident case (group [a]), three temporal controls (groups [b], [c] and [d]), and two spatial controls (groups [e] and [f]), as shown in Table 1.

Case group [a] represents the near-accident event, which is defined by the time segment of 10-s before the accident, namely from the 33rd to 43rd seconds, and based on the fast lane. Five control groups are on same stretch of road but at different periods and for different lanes. Each group has equal values in terms of time duration (10 s) and lane length (50 m). Therein, three temporal controls show the risk conditions of 20-s pre-accident (group [b]), 30-s pre-accident (group [c]) and 40-s pre-accident (group [d]), for the fast lane. Two spatial controls cover the risk conditions on adjacent lanes, namely the middle lane (group [e]) and the slow lane (group [f]), during the near-accident period.

Seven basic indicators are calculated on the basis of each case-control group, as shown in Table 1. For instance, in the Case [a], the 10-s traffic volume has the vehicle count of eight on the fast lane (defined by the 50-m segment), accordingly, risk assessment is based on the eight vehicles. Among the eight vehicles, one pair of vehicles crashed (Vehicle IDs: 26 and 27). Following vehicles after vehicle 27 are not taken into consideration, since at that juncture, the crash has already been initiated, and thus the pre-accident state is turned into a post-accident state.

One problem in existing indicators (e.g. TTC, DRAC) is how to determine the threshold values that are used to distinguish different risk levels. The definition of risk levels is threshold sensitive, determined by different thresholds. A serious exceedance of defined threshold indicates a high likelihood of an accident. However, standard threshold values have not been determined yet. Herein, a range of threshold values are used to test the impacts of different threshold values on risk assessment. Six TTC threshold values from 1.5 to 4.0 (seconds) are included for TET and TIT, benchmarked in previous studies (e.g. van der Horst, 1990; Mahmud et al., 2017). The DRAC threshold is 3.4 m/s^2 (Archer, 2005; Guido et al., 2010). Regarding CPI, MADR1 (only considering pavement surface conditions) and MADR2 (under the assumption of a truncated normal distribution) are applied (Cunto and Saccomanno, 2008; Guido et al., 2010). A deceleration rate of 3.3 (m/s^2) and 1.0 s reaction time are assumed in PICUD (Uno et al., 2003).

4.3. Indicator based risk assessment

Pre-accident risks are assessed by the seven basic indicators, each of which is useful in distinguishing risk levels in certain ways. According to Table 1, it is found that: (1) the performance of each indicator is different in measuring risks, therein, TIT and CPI are better in identifying accident risk conditions from the traffic flow; (2) TIT can identify many pre-accident risk conditions and CPI is helpful in further identifying the severest conditions (the near-accident) from among these risk conditions; (3) for the threshold issue, the impact of using different threshold values is not very critical in determining risk levels; and (4)

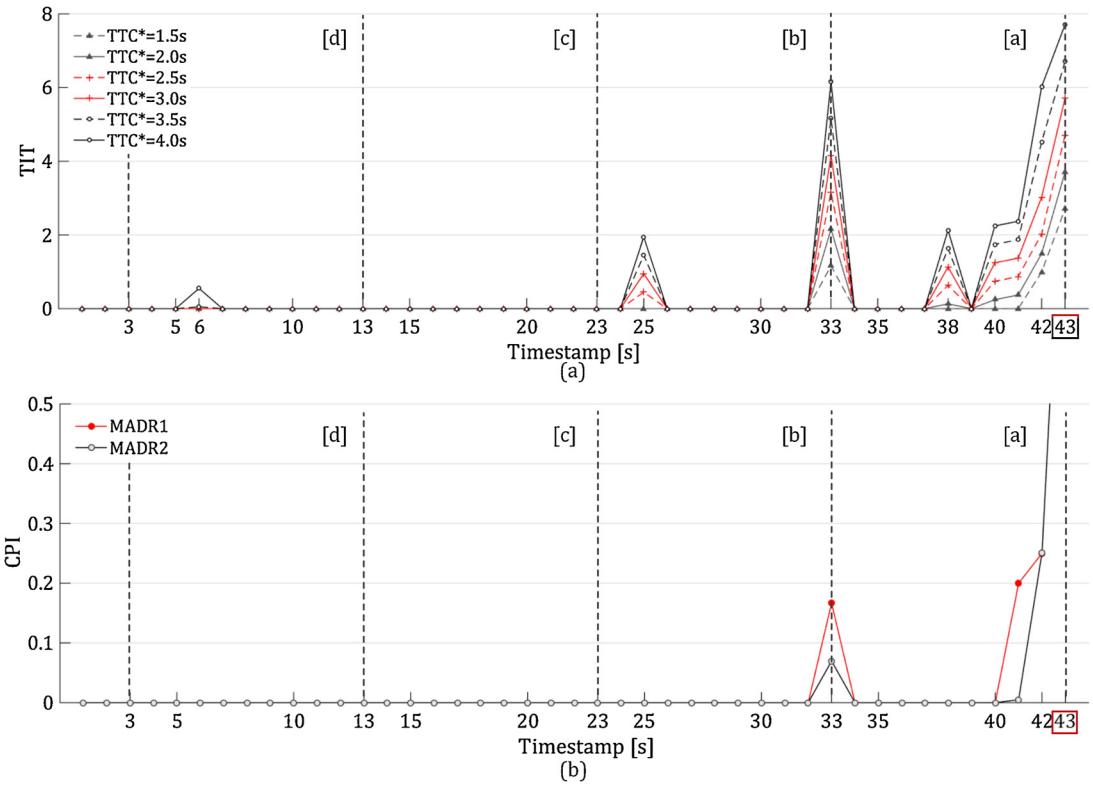

Fig. 4. Pre-accident risk assessment for the fast lane based on indicators.

PSD is helpful to describe the spatial proximity in emergency risks.

The lane-level risk assessment based on TIT and CPI are illustrated in Fig. 4(a) and (b).

From the TIT-time curve in Fig. 4(a), the lane-level pre-accident risk conditions are monitored, and TIT contributes to the identification of risk exposures from traffic flow, for example, around the 33rd and after the 37th seconds. A higher TTC threshold value (e.g. 4.0 s) is more sensitive in identifying risk conditions, while a critical threshold value (e.g. 1.5 s) is helpful to figure out the risk conditions with high severity. But the impact of different TTC threshold values is not very critical in determining the high-risk conditions.

Fig. 4(b) shows the serious risk exposures which are relatively difficult to avoid. Two serious risk conditions are identified by CPI, one of which closely match with the actual accident. Two CPI measures (i.e. MADR1 and MADR2) are found to be similar in figuring out the risk conditions. The near-accident or near-miss events could be estimated by CPI, including potential locations and timestamps in exposure to an accident.

Compared with the risk conditions suggested by TIT and CPI, there is an extensive identification of potential risks on the basis of distance-based indicators. PSD performs better in moderately identifying potential risks. Hence, PSD is introduced as complementary measurement for accident risks associated with potential emergencies, such as secondary accident in chain collisions.

4.4. Vehicle-level risk assessment

Risk exposures in terms of individual vehicles (vehicle pairs) are identified from vehicle TIT and CPI values, as shown in Fig. 5(a) and (b). From vehicle-TIT, the at-risk vehicles are able to be identified, especially the vehicles 24–27, which were involved in the accident. The vehicle crash avoidance performance is measured by CPI. The CPI can identify the vehicles with high-risk behaviours and which specific vehicles are likely to cause an accident, as shown in Fig. 5(b). Furthermore, TIT and CPI also characterise vehicle risks, which is potentially very useful, such as for driving behaviour analysis, insurance-based risk pricing, and targeted safety enhancement, etc.

4.5. KRIs as hybrid indicators

Following these findings, the concept of KRI is further enhanced, which is using hybrid and hierarchical indicators to distinguish risk levels with simplified threshold measurements. It is clear that indicator-based risk assessment is quantifiable, especially using TIT and CPI. TIT shows a general collision risk by vehicle conflicts, and CPI exhibits the identification of a higher risk severity, which tends to yield a higher likelihood of an accident. CPI and TIT are therefore used as the basic indicators to structure the hybrid and hierarchical KRIs, as well as PSD.

There are two main aspects for risk exposures, namely risk severity and the likelihood. The basic expression of KRI is proposed to measure the risk severity (S) with three levels, which are serious risk or high risk (SR), middle risk (MR) and low risk (LR), as follows:

$$KRI\ (S) = \begin{cases} LR: & CPI = 0 \quad \&TIT = 0 \quad \&PSD \le 1 \\ MR: & CPI = 0 \quad \&TIT > 0 \\ SR: & CPI > 0 \end{cases}$$

Note that $KRI\,(S)$ is calculated with respect to an individual vehicle or the entire vehicle stream for a specific time and road space. The risk levels of LR and MR are primarily determined by TIT values, where TIT = 0 corresponds to a risk with a low potential of accident, especially when $PSD \le 1$. CPI is then used to measure whether the risk is avoidable or not, which distinguishes the conflicts between MR conditions and SR events. The calculations of TIT and CPI are threshold-sensitive, which are evaluated based on the threshold values of TTC and

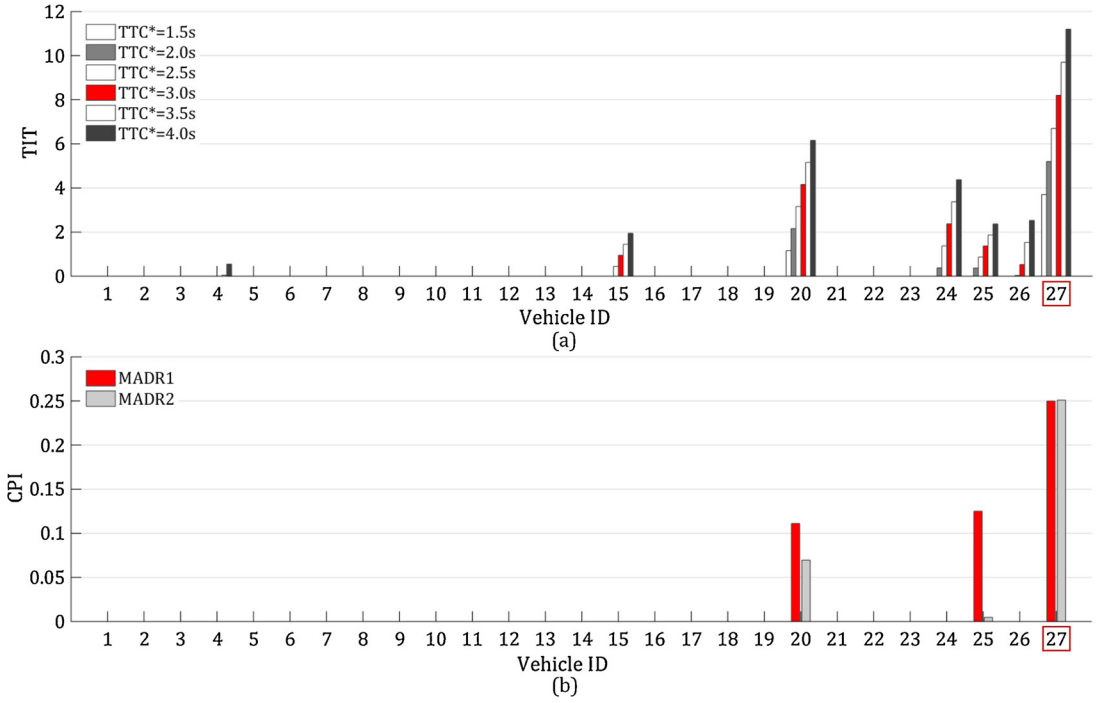

Fig. 5. Vehicle-level risk identification by indicators.

DRAC, respectively. Since the risk levels are distinguished by the hybridised KRI, the impact of different threshold values is not very critical. It is a new insight in measuring risk levels, which is also flexible in defining straightforward thresholds in determining risk levels.

The risk likelihood (L) is measured by the total time of different severity levels with respect to time period (T), defined as follows:

$$KRI(L) = \begin{cases} MR: \sum_{i=1}^{M} \sum_{t=0}^{N} \alpha_i(t) \cdot \tau_{sc} \\ SR: \sum_{i=1}^{M} \sum_{t=0}^{N} \beta_i(t) \cdot \tau_{sc} \end{cases}$$

$$\alpha_i(t) = \begin{cases} 1 & \forall \ TIT > 0 \ \& \ CPI = 0 \\ 0 & otherwise \end{cases}$$

$$\beta_i(t) = \begin{cases} 1 & \forall \ CPI > 0 \\ 0 & otherwise \end{cases}$$

where M is the entire vehicle stream in specific road space, τ_{sc} is a small-time interval ($T = N \cdot \tau_{sc}$), and $\alpha_i(t)$ and $\beta_i(t)$ are switching variables with value 1 and 0 for risk level judgement.

$KRI(L)$ measures the accumulation of vehicle-level risks and aggregation of flow-level risks for different severity levels. As a result, the likelihood can be used to describe risk exposures with different frequency levels, such as occasional, probable, frequent, etc. Therefore, $KRI(L)$ is meaningful to monitor the trends of risk exposures.

It is worthwhile to highlight that the risk assessment using KRI is based on the following assumptions that: (1) the higher severity of a risk condition or a vehicle behaviour, the more likely an accident will happen; (2) the harder a risk to be avoided by available evasive manoeuvres, the more likely an accident will happen; and (3) the more accumulation of vehicle-level risks or aggregation of flow-level risks, the more likely an accident will happen.

4.6. Validation

To further validate the concept of KRI, a second real-world accident case is examined. Detailed analysis of this accident for validation of KRI is provided in Appendix B, including accident description, KRI-based risk assessment with predefined thresholds, risk exposures in terms of traffic flow and individual vehicles, etc. The findings of the second accident provide supporting evidences that there are certain pre-accident risk conditions for which KRI-based risk assessment is helpful to determine such risk conditions with different levels. As consistent with the concept of KRI, the risk levels are distinguished by hybridised KRIs, and predefined threshold measurement is also workable. The results of the two accidents are in close agreements. Notwithstanding, for a proper and scientific evaluation of KRI, calibration and validation using more accident cases is still important, and this aspect is discussed in the discussion section.

5. Discussion

5.1. Applications

KRIs can identify pre-accident risk exposures in terms of severity and likelihood. Higher risk levels and frequency have predictive values and can act as early signals of accidents, and constant monitoring of KRIs is helpful for accident assessment and prediction. Combined with the forecasting of vehicle movements, the at-risk vehicles, locations and timestamps of potential accidents can be inferred in real-time. Therefore, targeted prevention could be applied pre-emptively. Furthermore, surrogate measures using KRIs are also helpful for risk-related analysis, such as risk data labelling, risk feature learning, risk pattern recognition. For example, the proposed KRI has been applied to label risk levels of vehicle driving data; and using feature learning to identify risk behaviours and make accident prediction (Shi et al., 2018).

5.2. Limitation

This study is a proof of concept of the KRI from an experimental standpoint. To get a stronger evaluation and validation, in-depth study using more accident cases is recommended. The scope of the technique can be extended by applying the method to additional real-world accidents cases, including various types of accidents and near-miss cases collected from expressways, intersections, arterial roads, etc. More

accident cases can be analysed to allow examination of the sensitivity and specificity, the false positive rates and false negative rates, and d-primed value, etc. In addition, appropriate threshold values can be defined to further subdivide risk levels. For instance, a possible subdivision of the SR-level could be extra serious risk or near-accident level when CPI > 0.5. Besides, there is a lack of leading indicators for accident prediction. Leading indicators should continue to be developed with the aim for proactive prevention with a lead time.

6. Conclusion

The risk assessment using hybrid and hierarchical indicators (the KRIs) offers new insights about risk exposures, which is helpful for accident assessment and prediction. This study assesses the feasibility of using KRIs to measure pre-accident risk exposures conditioned on real-world accident data. This research contributes to the literature in three areas.

First, the concept of KRI is formulated to assess risk exposures using hybrid indicators. Seven individual indicators are selected as the basic indicators of KRIs in terms of risk behaviour, risk avoidance, and risk margin. A temporal-spatial case-control study is designed to investigate the feasibility of each indicator with the key findings that TIT can identify many pre-accident risk conditions and CPI can pick out the severest conditions (the near-accident) from among these risk conditions. In addition, it is found that the impact of different threshold values is not very critical in determining risk levels.

Second, KRI uses hybrid indicators to hierarchically distinguish various risk levels. The expressions of KRIs have been developed mainly based on TIT and CPI, to measure risk severity with three levels, as well as the likelihood. It is also flexible in defining straightforward threshold values for classification of risk levels. The KRIs and their threshold measurements are then further validated by another independent accident case.

Last but not the least, a grid remapping method has been developed to obtain vehicle trajectory data from surveillance video system, which can be applied for coordinate transformation from image pixels to real-world units with a high quality. In addition, two real-world accident events and their antecedent (pre-crash) road traffic movements are retrieved, which unveils some insights of pre-accident risks.

Acknowledgements

This study is conducted as part of first author's PhD research project. The study is supported by Singapore Ministry of Education Academic Research Fund Tier 2MOE2013-T2-2-073 and MOE2014-T2-2-097. The authors thank the Land Transport Authority for providing the surveillance video footages of the accident events. The authors thank the two anonymous reviewers whose insights and suggestions lead to a big improvement of this paper and open up new directions for further studies. All remaining errors, if any, are the authors' responsibilities.

Appendix A. Terminologies of Surrogate Risk Indicators

Acronym	Definition	Explanation	References
CPI	Crash Potential Index	The probability that a given vehicle DRAC exceeds its maximum available deceleration rate (MADR) or braking capability during a given time interval	Cunto and Saccomanno (2008)
DRAC	Deceleration Rate to Avoid Crash	Differential speed between a following vehicle and corresponding lead vehicle divided by closing time	Almqvist et al. (1991)
MADR	Maximum Available Deceleration Rate	Braking capacity defined by several factors	Cunto and Saccomanno (2008)
PICUD	Potential Index for Collision with Urgent Deceleration	The distance between two consecutive vehicles when they abruptly break and stop completely	Uno et al. (2003)
PSD	Proportion of Stopping Distance	The ratio of the remaining distance to the potential collision point and the minimum acceptable stopping distance	Allen et al. (1978)
TET	Time Exposed TTC	The length of time a TTC-event remains below a designated TTC-threshold	Minderhoud and Bovy (2001)
TIT	Time Integrated TTC	The integral of the TTC-profile during the time below the threshold	Minderhoud and Bovy (2001)
TTC	Time to Collision	The time until a collision between two vehicles would have occurred if the collision course and speed difference are maintained	van der Horst (1990)

Appendix B. Analysis of Second Accident Case for Validation of KRI

An independent real-world accident is examined to further validate the concept of KRI. The second accident was also a head-to-rear collision that occurred on the fastest lane of an expressway carriageway during mid-afternoon. The road segment with grid remapping is shown in Fig. B1(a). The traffic scenario at the time of accident is provided in Fig. B1(b). At the 44th second, the vehicle with pixel coordinates (894, 409) was hit by a following vehicle, which thus led to a multi-vehicle collision. Similarly, the 40-s pre-accident vehicle trajectory data are extracted from video images and transformed into real-world units.

Based on the proposed KRIs, the risk levels of SR, MR and LR are determined. The risk conditions of MR-level and SR-level are figured out, using straightforward threshold measurement that CPI > 0 for SR and TIT > 0 for MR. TTC threshold is 4.0 s for TIT calculation, and CPI value is the average of two results calculated based on MADR1 and MADR2 respectively. KRI-based risk assessment for traffic flow (defined by vehicle counts per 0.5 s for the fast-lane segment) is provided in Fig. B2(a), and KRI-based vehicle-level risk assessment is provided in Fig. B2(b).

In Fig. B2(a), the risk exposures in terms of traffic flow are identified, including risk severity and duration, the trends of risk aggregation, etc. There are two SR-level risk conditions (the 35th–40th seconds, and after the 42nd second), which are determined by the aggregated CPI values. From a temporal comparison, most of the identified higher-risk conditions are presented during the period of 10-s before the time of accident occurrence. In addition, the trends of risk aggregation are also provided in Fig. B2(a). The direction and range of risk trends can be used as early signals to infer accident likelihood. Herein, these findings provide supporting evidences that there are certain pre-accident risk conditions for which KRI-based risk assessment is helpful to identify such risk conditions.

The vehicle-level risk exposures are also identified by KRIs, as shown in Fig. B2(b). KRI-based vehicle risk assessment also reveals many insights about risk information in the vehicle stream, including at-risk vehicles (vehicle-pairs), risk accumulation within individual vehicles, and risk portrayal among vehicles, etc. From the vehicle with ID 17, the accumulations of MR-level risks have a growing trend and conduct within vehicle platoons. Similarly, SR-level risk portrayal is also exhibited from the vehicle with ID 23. Therefore, the risk accumulation and portrayal can be used to infer the most-at-risk vehicles.

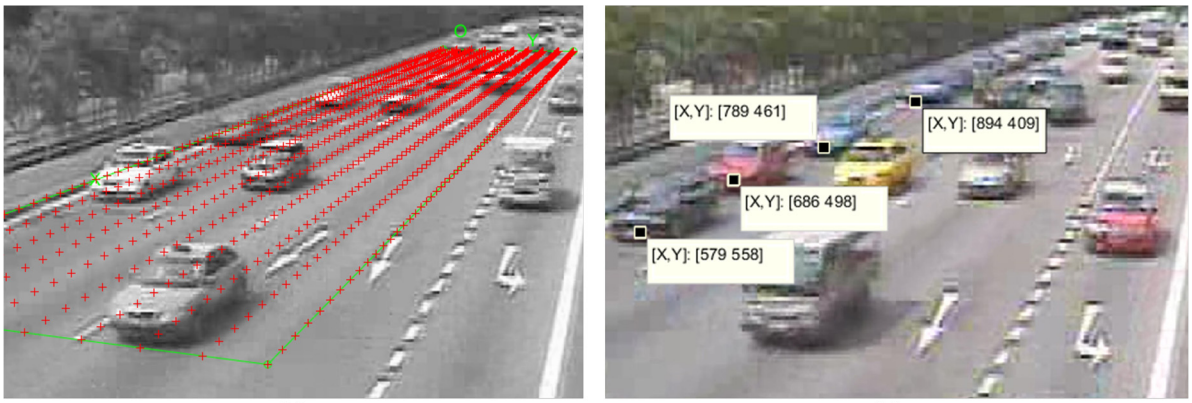

Fig. B1. Road segment with grid remapping and data extraction.

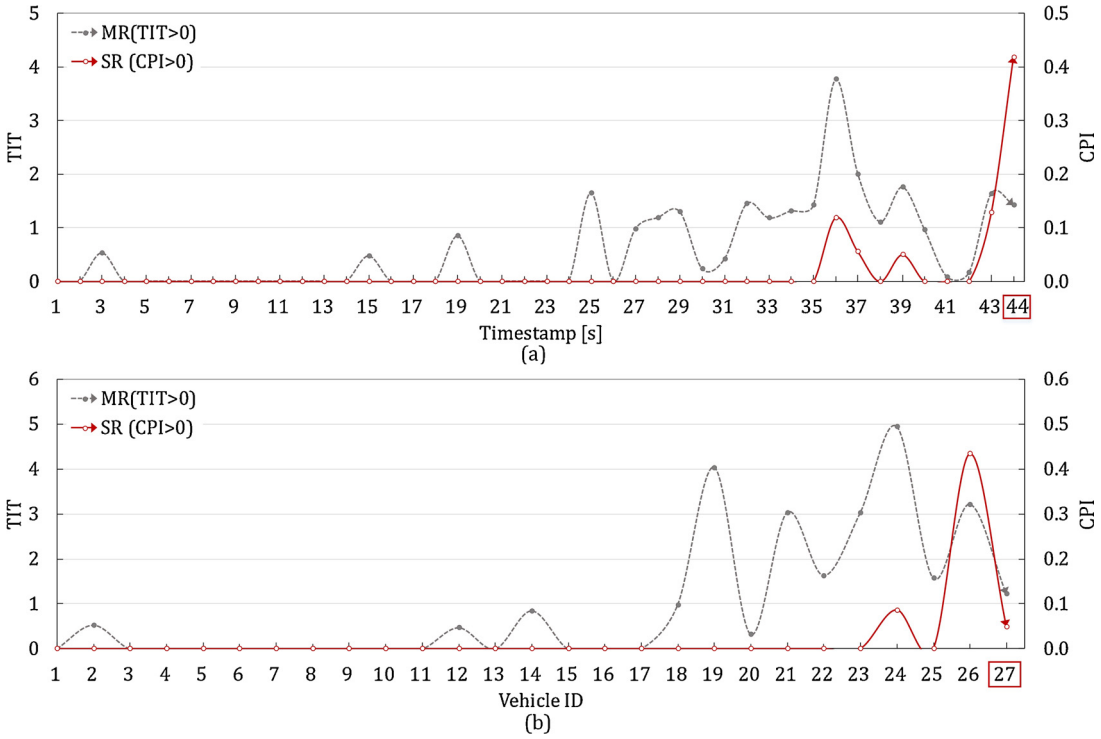

Fig. B2. KRI-based pre-accident risk assessment.

However, more details about near-accident events were not well captured in the second accident. The main reason is that the accident occurred at the far-ground of the remapping area, which is thus not conducive for observation and data collection. In addition, the time span of near-accident duration was relatively much shorter.

References

Abdel-Aty, M., Haleem, K., 2011. Analyzing angle crashes at unsignalized intersections using machine learning techniques. Accid. Anal. Prev. 43 (1), 461–470.

Allen, B.L., Shin, B.T., Cooper, P.J., 1978. Analysis of traffic conflicts and collisions. Transp. Res. Rec. 667, 67–74.

Almqvist, S., Hydén, C., Risser, R., 1991. Use of speed limiters in cars for increased safety and a better environment. Transp. Res. Rec. (1318), 34–39.

Amundsen, F.H., Hydén, C., 1977. In: Proceeding of First Workshop on Traffic Conflicts. Institute of Transport Economics, Oslo/Lund Institute of Technology, Oslo, Norway.

Archer, J., 2005. Indicators for traffic safety assessment and prediction and their application in micro-simulation modelling: a study of urban and suburban intersections. Doctoral Dissertation. KTH Royal Institute of Technology.

Chai, C., Wong, Y.D., 2013. Automatic vehicle classification and tracking method for vehicle movements at signalized intersections. IEEE Intelligent Vehicles Symposium (IV). pp. 624–629.

Chai, C., Wong, Y.D., 2015. Comparison of two simulation approaches to safety assessment: cellular automata and SSAM. J. Transp. Eng. 141 (6), 05015002.

Chai, C., Wong, Y.D., Wang, X., 2017. Safety evaluation of driver cognitive failures and driving errors on right-turn filtering movement at signalized road intersections based on Fuzzy Cellular Automata (FCA) model. Accid. Anal. Prev. 104, 156–164.

Chin, H.C., Quek, S.T., 1997. Measurement of traffic conflicts. Saf. Sci. 26 (3), 169–185.

Cunto, F.J.C., Saccomanno, F.F., 2008. Calibration and validation of simulated vehicle safety performance at signalized intersections. Accid. Anal. Prev. 40 (3), 1171–1179.

Dong, N., Huang, H., Zheng, L., 2015. Support vector machine in crash prediction at the level of traffic analysis zones: assessing the spatial proximity effects. Accid. Anal. Prev. 82, 192–198.

El-Basyouny, K., Sayed, T., 2013. Safety performance functions using traffic conflicts. Saf. Sci. 51 (1), 160–164.

Guido, G., Saccomanno, F., Vitale, A., Astarita, V., Festa, D., 2010. Comparing safety performance measures obtained from video capture data. J. Transp. Eng. 137 (7), 481–491.

Hakkert, A.S., Gitelman, V., 2014. Thinking about the history of road safety research: past achievements and future challenges. Transp. Res. Part F 25, 137–149.

Hormann, K., Agathos, A., 2001. The point in polygon problem for arbitrary polygons. Comput. Geom. 20 (3), 131–144.

Hwang, S., Fraser, J., Simkins, B.J., 2010. Identifying and communicating key risk indicators. Enterp. Risk Manage. 125–140.

Imprialou, M., Quddus, M., 2017. Crash data quality for road safety research: current state and future directions. Accid. Anal. Prev. http://dx.doi.org/10.1016/j.aap.2017.02.022.

Laureshyn, A., Svensson, Å., Hydén, C., 2010. Evaluation of traffic safety, based on micro-level behavioural data: theoretical framework and first implementation. Accid. Anal. Prev. 42 (6), 1637–1646.

Mahmud, S.S., Ferreira, L., Hoque, M.S., Tavassoli, A., 2017. Application of proximal surrogate indicators for safety evaluation: a review of recent developments and research needs. IATSS Res. http://dx.doi.org/10.1016/j.iatssr.2017.02.001.

Mannering, F.L., Shankar, V., Bhat, C.R., 2016. Unobserved heterogeneity and the statistical analysis of highway accident data. Anal. Methods Accid. Res. 11, 1–16.

Minderhoud, M.M., Bovy, P.H., 2001. Extended time-to-collision measures for road traffic safety assessment. Accid. Anal. Prev. 33 (1), 89–97.

Saifuzzaman, M., Zheng, Z., 2014. Incorporating human-factors in car-following models: a review of recent developments and research needs. Transp. Res. Part C 48, 379–403.

Scandizzo, S., 2005. Risk mapping and key risk indicators in operational risk management. Econ. Notes 34 (2), 231–256.

Sivaraman, S., Trivedi, M.M., 2013. Looking at vehicles on the road: a survey of vision-based vehicle detection, tracking, and behavior analysis. IEEE Trans. Intell. Transp. Syst. 14 (4), 1773–1795.

Shi, X., Wong, Y.D., Li, M.Z.F., Chai, C., 2018. Accident risk prediction based on driving behavior feature learning using CART and XGBoost. Transportation Research Board 97th Annual Meeting, No. 18-06270.

Sobhani, A., Young, W., Sarvi, M., 2013. A simulation based approach to assess the safety performance of road locations. Transp. Res. Part C 32, 144–158.

Uno, N., Iida, Y., Yasuhara, S., Suganuma, M., 2003. Objective analysis of traffic conflict and modeling of vehicular speed adjustment at weaving section. Infrastruct. Plann. Rev. 20 (4), 989–996.

van der Horst, A.R.A., 1990. A time-based analysis of road user behaviour in normal and critical encounters. Doctoral Dissertation. Delft University of Technology No. HS-041 255.

Wang, J., Zhang, L., Zhang, D., Li, K., 2013. An adaptive longitudinal driving assistance system based on driver characteristics. IEEE Trans. Intell. Transp. Syst. 14 (1), 1–12.

Wu, K.F., Aguero-Valverde, J., Jovanis, P.P., 2014. Using naturalistic driving data to explore the association between traffic safety-related events and crash risk at driver level. Accid. Anal. Prev. 72, 210–218.

Young, R.A., 2017. Talking on a wireless cellular device while driving: improving the validity of crash odds ratio estimates in the SHRP 2 naturalistic driving study. Safety 3 (4), 28.

Zhang, Z., 2000. A flexible new technique for camera calibration. IEEE Trans. Pattern Anal. Mach. Intell. 22 (11), 1330–1334.

Zhang, Z., 2004. Camera calibration with one-dimensional objects. IEEE Trans. Pattern Anal. Mach. Intell. 26 (7), 892–899.

Zheng, L., Ismail, K., Meng, X., 2014. Traffic conflict techniques for road safety analysis: open questions and some insights. Can. J. Civil Eng. 41 (7), 633–641.